Available online at www.sciencedirect.com
SCIENCE DIRECT®
Scripta Materialia 50 (2004) 243–248
Scripta MATERIALIA
www.actamat-journals.com

Comparison of high temperature shape memory behaviour for ZrCu-based, Ti–Ni–Zr and Ti–Ni–Hf alloys

G.S. Firstov [a,b,*], J. Van Humbeeck [a], Yu.N. Koval [b]

[a] Department of Metallurgy and Materials Engineering, Catholic University of Leuven, Kasteelpark Arenberg 44, B-3001 Leuven, Belgium
[b] Institute of Metal Physics of the National Academy of Sciences of Ukraine, 36 Vernadsky str. 03142, Kiev-142, Ukraine

Accepted 4 September 2003

Abstract

New ZrCu-based high temperature shape memory alloys with M_s close to 500 K are under development. The shape memory behaviour of this material is compared to those of Ti–Ni–Zr and Ti–Ni–Hf alloys. The optimal compositions show a shape recovery of not less than 3% at temperatures above 470 K.

Keywords: Martensitic phase transformation; Shape memory alloys; High temperature shape recovery

1. Introduction

A number of potentially high temperature shape memory alloys have been investigated so far [1–4]. Amongst them, still, Ti–Ni–Zr and Ti–Ni–Hf alloys are studied most significantly, mainly because of the relative low prices for the raw materials. In this regard, the Zr-based quasi-binary intermetallics also can be considered competitive, as they appeared to show quite high temperatures of martensitic transformation (MT) associated with a decent high temperature shape memory effect [5–7]. The aim of the present paper is to study ZrCu-based, Ti–Ni–Zr and Ti–Ni–Hf alloys, with similar MT temperatures in order to compare their high temperature shape memory potential.

2. Experimental

Zr–Cu–Ni–Co–Ti, Ti–Ni–Zr and Ti–Ni–Hf alloys were arc-melted from iodide Ti, Zr and Hf and electrolytic Co, Ni and Cu in a pre-gettered argon atmosphere and poured into a water-cooled copper mould. MT temperatures were detected with the help of TA 2920 differential scanning calorimeter using a heating-cooling rate of 5 K/min. Shape recovery was examined in a TMA 934 dilatometer using a 5 K/min heating-cooling rate after compression at a rate of 2.8×10^{-3} s^{-1} in an INSTRON 1196 equipped with furnace.

3. Results

During the extensive study [8] of the three groups of alloys under consideration, four alloys with the optimal shape recovery were chosen (Table 1, Figs. 1 and 2), taking into account the fact that their reverse MT temperatures are higher than 390 K (definition of a high temperature shape memory alloy proposed in [3]).

Deformation prior to shape recovery was applied at room temperature (Figs. 3 and 4, thin lines) and after in-situ heating above reverse MT finish temperature A_f and subsequent cooling to forward MT start temperature M_s (Figs. 3 and 4, thick lines).

It can be seen that $ZrCu_{28.2}Ni_{6.8}Co_{15.4}$ exhibits strong parabolic strain hardening at room temperature (Fig. 3, Table 2). Ti additions ($ZrCu_{29.9}Ni_{11}Co_{10.2}Ti_{6.6}$ alloy, Fig. 3, Table 2) change the strain hardening at room temperature from parabolic to less intensive linear. A superelastic effect of about 1.9% strain on unloading is visible (Fig. 3, thin line). Compression of $ZrCu_{28.2}Ni_{6.8}Co_{15.4}$ at M_s is followed by linear strain hardening, which

* Corresponding author. Address: Department of Metallurgy and Materials Engineering, Catholic University of Leuven, Kasteelpark Arenberg 44, B-3001 Leuven, Belgium. Tel.: +32-16-321448; fax: +32-16-321992.
E-mail address: georgiy.firstov@mtm.kuleuven.ac.be (G.S. Firstov).

1359-6462/$ - see front matter
doi:10.1016/j.scriptamat.2003.09.010

Table 1
Heat exchange and temperatures for thermally induced MT in ZrCu- and TiNi-based SMAs with maximal shape recovery (ε_R)

Composition (at.%)	M_s (K)	M_f (K)	A_s (K)	A_f (K)	$Q^{A>M}$ (J/mol)	$Q^{M>A}$ (J/mol)	E_d (J/mol)	ε_R (%)
$ZrCu_{28.2}Ni_{6.8}Co_{15.4}$	520	400	485	600	1318	1524	206	2.5
$ZrCu_{29.9}Ni_{11}Co_{10.2}Ti_{6.6}$	450	340	410	520	1156	1230	74	3.5
$TiNi_{48.78}Zr_{18.21}$	490	410	470	550	1569	1630	61	3.7
$TiNi_{49.42}Hf_{14.63}$	460	380	435	510	1750	1837	87	3.4

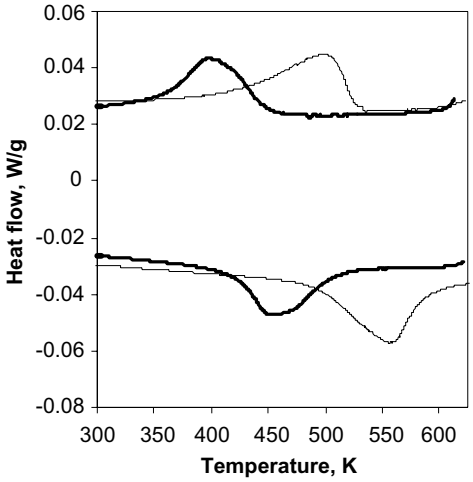

Fig. 1. DSC measurements of the complete MT cycle for $ZrCu_{28.2}Ni_{6.8}Co_{15.4}$ (thin line) and $ZrCu_{29.9}Ni_{11}Co_{10.2}Ti_{6.6}$ (thick line) alloys.

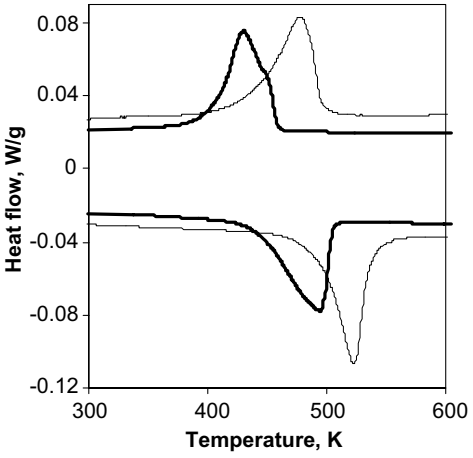

Fig. 2. DSC measurements of the complete MT cycle for $TiNi_{48.78}Zr_{18.21}$ (thin line) and $TiNi_{49.42}Hf_{14.63}$ (thick line) alloys.

is strong but less intensive than the room temperature case ($d\sigma/d\varepsilon = 10.7$ GPa). The stress–strain behaviour of the $ZrCu_{29.9}Ni_{11}Co_{10.2}Ti_{6.6}$ during compression at M_s is more complex (Fig. 3, thick line, Table 2). Two stages of the deformation are visible. 1.4% of superelastic deformation (ε_{SE}) was restored on unloading.

Strong parabolic strain hardening at room temperature is similar for both TiNi-based alloys (Fig. 4, thin lines). The compression at M_s for $TiNi_{48.78}Zr_{18.21}$ alloy

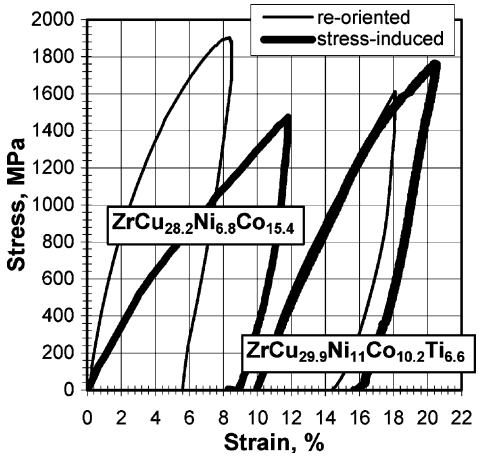

Fig. 3. Stress–strain behaviour in compression detected at room temperature (thin line) and after in-situ heating above A_f temperature and subsequent cooling to M_s temperature (thick line) for ZrCu-based alloys. Data for $ZrCu_{29.9}Ni_{11}Co_{10.2}Ti_{6.6}$ are shifted along strain axis by 10%.

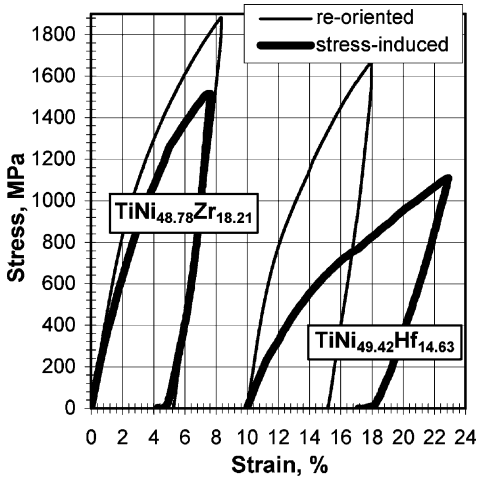

Fig. 4. Stress–strain behaviour in compression detected at room temperature (thin line) and after in-situ heating above A_f temperature and subsequent cooling to M_s temperature (thick line) for $TiNi_{48.78}Zr_{18.21}$ and $TiNi_{49.42}Hf_{14.63}$ alloys. Data for $TiNi_{49.42}Hf_{14.63}$ are shifted along strain axis by 10%.

did not result in any qualitative changes in stress–strain behaviour (Fig. 4, thick line, Table 2). As for $TiNi_{49.42}Hf_{14.63}$, the compression at M_s results in much lower yield strength and linear strain hardening with the lower

Table 2
Stress–strain and shape recovery parameters, volume change during MT and temperatures of shape recovery for ZrCu- and TiNi-based SMAs

Composition (at.% compression temp.)	σ_{02} (MPa)	$d\sigma/d\varepsilon$ (GPa)	ε_{SE} (%)	ε'_R (%)	ε''_R (%)	$\Delta V/V$ (%)	A'_s (K)	A''_s (K)
$ZrCu_{28.2}Ni_{6.8}Co_{15.4}$								
Room temperature	717	39–2ε	–	–	1.5	0.14	–	670
M_s (520 K)	590	10.7	1.2	0.6	1.8		540	640
$ZrCu_{29.9}Ni_{11}Co_{10.2}Ti_{6.6}$								
Room temperature	560	17.5	1.9	1.3	1.5		490	670
M_s (450 K)						0.13		
First stage	590	18.8	1.4	1.7	1.6		450	640
Second stage	1280	10.3	–					
$TiNi_{48.78}Zr_{18.21}$								
Room temperature	860	29–1.3ε	–	2	0.8	0.06	560	875
M_s (490 K)	580	32–1.7ε	1	3.1	1.1		520	$\leqslant$720
$TiNi_{49.42}Hf_{14.63}$								
Room temperature	680	25–0.9ε	–	2.4	–	0.03	510	>950
M_s (460 K)	304	6.1	1.2	3.1	0.8		475	820

rate $d\sigma/d\varepsilon = 6.1$ GPa. Superelasticity of 1.2% strain can be also noticed (Fig. 4, thick line).

The results of the thermal shape recovery measurements are shown in Figs. 5–8. It can be seen, that for $ZrCu_{28.2}Ni_{6.8}Co_{15.4}$ alloy after deformation at room temperature a shape recovery of 1.5% takes place in one step that starts at 670 K (Fig. 5, thin line). Deformation at M_s temperature results in a two-step shape recovery (Fig. 5, thick line, Table 2). Ti additions ($ZrCu_{29.9}Ni_{11}Co_{10.2}Ti_{6.6}$ alloy, Fig. 6) lead to an increase in two-step shape recovery. High temperature shape recovery stage has the same start temperature as $ZrCu_{28.2}Ni_{6.8}Co_{15.4}$.

TiNi-based alloys also show two-stage recovery (Figs. 7 and 8), although the high temperature stage is not so clearly defined as it can be seen for $ZrCu_{29.9}Ni_{11}Co_{10.2}Ti_{6.6}$. Temperatures of the shape recovery and recovered deformation were also obtained from the data presented in Figs. 7 and 8. As a result, it was possible to summarize all stress–strain and shape recovery parameters, volume change during MT and temperatures of shape recovery for all alloys in question (Table 2).

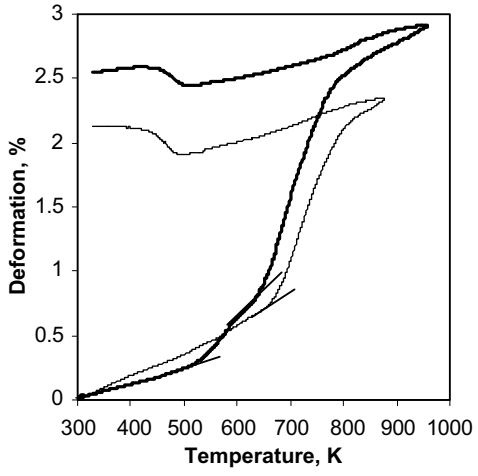

Fig. 5. High temperature shape recovery measured in the dilatometer after compression at room temperature (thin line) and after in-situ cooling from the austenitic state to M_s (thick line) for $ZrCu_{28.2}Ni_{6.8}Co_{15.4}$.

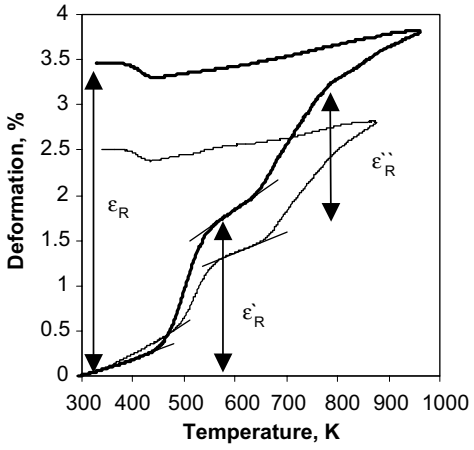

Fig. 6. High temperature shape recovery measured in the dilatometer after compression at room temperature (thin line) and after in-situ cooling from the austenitic state to M_s (thick line) for $ZrCu_{29.9}Ni_{11}Co_{10.2}Ti_{6.6}$.

4. Discussion

According to [9], non-thermoelastic MT in ZrCu intermetallic compound proceeds through the sequence of alternating $B2 \rightarrow B19'$ and $B2 \rightarrow Cm$ steps starting mainly from B19′ martensite (twinless) and completing by the preferential formation of the monoclinic martensite belonging to Cm space group (twinned). It can be

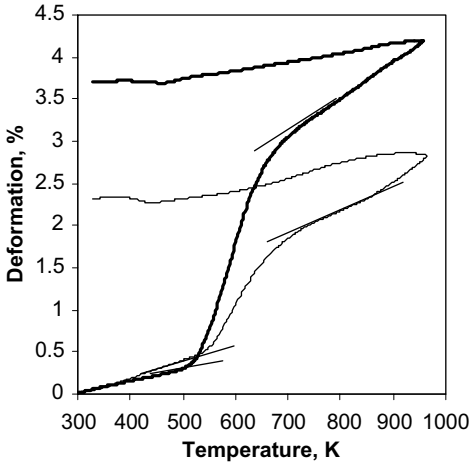

Fig. 7. High temperature shape recovery measured in the dilatometer after compression at room temperature (thin line) and after in-situ cooling from the austenitic state to M_s (thick line) for $TiNi_{48.78}Zr_{18.21}$.

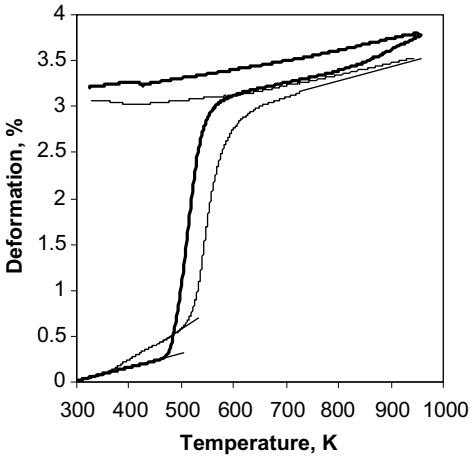

Fig. 8. High temperature shape recovery measured in the dilatometer after compression at room temperature (thin line) and after in-situ cooling from the austenitic state to M_s (thick line) for $TiNi_{49.42}Hf_{14.63}$.

seen (Fig. 1) that MT in ZrCu-based alloys under consideration is also taking place through two steps. However, in contrast to ZrCu [9], MT in $ZrCu_{28.2}Ni_{6.8}Co_{15.4}$ alloy shows already some signs of thermoelastic behaviour (smaller hysteresis, $A_s < M_s$; Fig. 1 (thin line), Table 1). Still, the energy Ed dissipated during the MT cycle ($E_d = Q^{M>A} - Q^{A>M}$, according to [10], where $Q^{M>A}$—the heat of the reverse MT, while $Q^{A>M}$—the heat of the forward one; Table 1) is high as well as the MT temperature intervals, when compared to TiNi-based alloys (Fig. 2, Table 1). From the shape of the calorimetric peaks (Fig. 1, thin line) it can be deduced that, similar to Zr_2CuNi–Zr_2CuCo quasi-binary cross-section [6], quaternary Co additions promote the formation of the B19′ martensite, which is forming first [9]. MT in $ZrCu_{29.9}Ni_{11}Co_{10.2}Ti_{6.6}$ alloy (Fig. 1, thick line) shows that Ti additions initiate the preferential formation of monoclinic martensite belonging to Cm space group, while still some amount of B19′ martensite is forming first on cooling. Disappearance of the Cm martensite at first on heating also can testify indirectly as another sign of thermoelastic behaviour because the thermoelasticity concept includes such requirement that the last portions of martensite phase on forward MT must be transformed to austenite in a first-order. The energy dissipated during MT in $ZrCu_{29.9}Ni_{11}Co_{10.2}Ti_{6.6}$ alloy is even smaller than for $TiNi_{49.42}Hf_{14.63}$ alloy but MT temperature intervals are still larger (Table 1) due to the specific formation of two martensitic phases. It also should be noted that the driving force of the MT is the highest for $TiNi_{49.42}Hf_{14.63}$, while the smallest one can be noticed for $ZrCu_{29.9}Ni_{11}Co_{10.2}Ti_{6.6}$ alloy (Table 1).

The value of the maximal shape recovery (ε_R) restored after heating and cooling back to room temperature, correlates well with the dissipated energy E_d (Table 1). The biggest overall shape recovery corresponds to the smallest E_d in the case of $TiNi_{48.78}Zr_{18.21}$. On the other hand, the shape recovery on heating shows more peculiar features (Figs. 5–8, Table 2). In the case of $TiNi_{49.42}Hf_{14.63}$, the high temperature shape recovery starting temperature A'_s (Table 2) is higher than A_s (Table 1) only by 30 and 75 K, respectively, when predeformed at M_s and room temperature. Such required overheating ($A'_s - A_s$) is larger (50 and 90 K) in $TiNi_{48.78}Zr_{18.21}$, while in the case of $ZrCu_{29.9}Ni_{11}Co_{10.2}Ti_{6.6}$ it is just in between (40 and 80 K). For $ZrCu_{28.2}Ni_{6.8}Co_{15.4}$, $A'_s - A_s = 65$ K after room temperature deformation. In other words, the martensite stabilization induced by the preliminary deformation is highest for $ZrCu_{28.2}Ni_{6.8}Co_{15.4}$ and smallest for $TiNi_{49.42}Hf_{14.63}$. Taking into account the stress–strain data (Figs. 3 and 4, Table 2) and the results presented for TiNiHf in [11], it can be supposed that such stabilization can be produced by the dislocation slip, which is accompanying the re-orientation of the thermally induced martensite (room temperature deformation, Figs. 3 and 4, thin lines, Table 2) and stress-induced MT (M_s deformation, Figs. 3 and 4, thick lines, Table 2).

The authors of [11] observed linear strain hardening during the stress-induced MT well over M_s, explaining it in terms of the martensitic deformation in combination with dislocation slip with the [1 0 0] (0 0 1) slip system. It was shown [12] that the critical stress for dislocation slip of the parent phase is almost the same as for the stress-induced MT. In our case, we deformed austenite at exactly M_s in order to achieve the best shape recovery possible. It can be seen that irreversible deformation associated with the dislocation slip was not avoided. Indeed, the preliminary deformation of $TiNi_{49.42}Hf_{14.63}$ was 8% (Fig. 4, thick line). The overall recovered one (ε_R) was only 3.4% (Fig. 6, Table 1). The same is applicable to TiNiZr and ZrCu-based alloys because of the

similar MT crystallography [13,14] with the only difference that (i) the strain hardening is more intensive and (ii) for $TiNi_{48.78}Zr_{18.21}$ it is already parabolic. It should be noted that in all cases of deformation at M_s, 1–1.4% of deformation was restored upon unloading (Table 2).

Reorientation of the thermally induced martensite of TiNi-based alloys and $ZrCu_{28.2}Ni_{6.8}Co_{15.4}$ during room temperature deformation is even more likely to be accompanied by dislocation slip because of the even more intensive parabolic strain hardening. Nevertheless, linear strain hardening at room temperature for $ZrCu_{29.9}Ni_{11}Co_{10.2}Ti_{6.6}$ results in a larger value of superelastic recovery (Table 2, Fig. 3). It is possible that internal twinning of the Cm martensite in addition to reorientation of martensite crystals promoted the superelastic behaviour compared to the twinless B19′ martensite, which is forming preferentially in $ZrCu_{28.2}Ni_{6.8}Co_{15.4}$.

After the first stage of shape recovery on heating a second stage is observed. For ZrCu-based alloys the starting temperatures of this stage (A_s'') coincide for room temperature and M_s deformation (670 and 640 K, respectively, Table 2). Taking into account that the martensite stabilization is caused by dislocation slip, let us assume that the second stage of the shape recovery is associated with heavily deformed martensite. Its eventual reversible movement is possible only in the case when the processes of the austenite nucleation and growth are still suppressed but recrystallization is already possible. Indeed, if we take into account the melting temperature of ZrCu-based alloys in question ($T_m = 1280$ K, [8]), the recrystallization temperature will then be $T_{re} = 0.5T_m = 640$ K, which is the same as A_s'' for both ZrCu-based alloys (Table 2, Figs. 5 and 6) predeformed at M_s. Once recrystallization starts, the forest of the dislocations formed during the deformation begins to disappear. Subsequently, destabilized martensite crystals instigate the high temperature shape recovery stage. In fact, the A_s'' temperature represents the temperature of recrystallization, which is slightly higher for the case of room temperature deformation but the same for both alloys, since their melting temperatures are the same. Such reasoning is valid for TiNi-based alloys as well. We measured their melting temperatures [8] and found them to be 1380 and 1440 K for $TiNi_{48.78}Zr_{18.21}$ and $TiNi_{49.42}Hf_{14.63}$, respectively. This means the recrystallization temperature for $TiNi_{48.78}Zr_{18.21}$ is about $0.52T_m$, while we have $0.57T_m$ in the case of $TiNi_{49.42}Hf_{14.63}$ pre-deformed at M_s (Table 2). More severe room temperature deformation increases the recrystallization temperatures for $TiNi_{48.78}Zr_{18.21}$ up to $0.63T_m$, while for $TiNi_{49.42}Hf_{14.63}$ it was higher than 0.66Tm, which was beyond our experimental possibilities.

An argument for the above mentioned mechanism of the high temperature shape recovery far beyond the reverse MT is the fact that after cooling to room temperature after shape recovery, the forward MT volume effect is visible at nominal MT (Figs. 5–8, Table 1). This implies that most of the internal dislocation substructure formed during the deformation is no longer present.

It has to be noted that the most attractive material is $TiNi_{49.42}Hf_{14.63}$, because its first stage shape recovery, associated with the reverse MT, has the narrowest temperature interval and the larger amount of 3.1% of the shape recovery at this stage. Taking into account the deformation recovered by recrystallization processes, it is clear that about 0.8% of the recoverable strain can be added to the existing amount if the necessary strengthening to avoid plastic deformation by slip can be achieved. The same is true for $TiNi_{48.78}$ $Zr_{18.21}$, where the maximal overall shape recovery was achieved (Table 1). Additional strengthening of some kind should narrow the temperature intervals of shape recovery and add more than 1% of the recoverable deformation to the existing one.

As for ZrCu-based alloys, where the maximal overall shape recovery after room temperature deformation was achieved (Table 2), it is clear that preferential (or only) formation of Cm martensite can improve the shape recovery of this material. Thus, in case only Cm martensite is formed and no plastic deformation occurs, the shape memory effect for ZrCu-based alloys can be improved and probably even compared with the behaviour of Ti–Ni–Hf. On the other hand, once Ti–Ni–Zr and Ti–Ni–Hf compositions have exhausted their potential in a sense of further increase of the temperatures of shape recovery, ZrCu-based alloys can be adjusted easily up to 1000–1100 K by alloying [7]. Ultra high temperatures of shape recovery, similar to those of ZrCu-based alloys, can be achieved only for a few very expensive HTSMA [1–5].

5. Conclusions

- The stress–strain behaviour during compression of high temperature shape memory alloys in question is characterized by the high strain hardening associated with the plastic deformation by the dislocation slip.
- Dislocation slip is responsible for the stabilization of re-oriented and stress-induced martensite.
- Martensite stabilization results in the two-stage shape recovery on heating. The high temperature stage is associated with the reverse transformation of plastically deformed martensite, instigated by recrystallization processes.
- The critical requirement for optimal high temperature shape memory behaviour is avoiding plastic deformation during pre-straining.
- High temperature shape memory alloys in question undergo thermoelastic martensitic transformation

but do not perform yet as well-established NiTi alloys at lower temperatures.

References

[1] Beyer J, Mulder JH. Proceedings of Advanced Materials'93, Transactions of Material Research Society, Japan 1994;18B:1003–8.
[2] Fonda RW, Jones HN, Vandermeer RA. Scr Mater 1998;39(8):1031–7.
[3] Van Humbeeck J. Trans ASME J Eng Mater Technol 1999;121:98–101.
[4] Otsuka K, Ren X. Intermetallics 1999;7:511–28.
[5] Koval YuN, Firstov GS, Van Humbeeck J, Delaey L, Jang WY. J Phys IV C8 1995;5:1103–8.
[6] Firstov GS, Koval YuN, Van Humbeeck J. J Phys IV C5 1997; 7:549–54.
[7] Firstov GS, Van Humbeeck J, Koval YuN. In: Proceedings of SMST'99, CD SMST-99. Shape Memory And Superelastic Technologies, SMST Europe; 1999. p. 446–50.
[8] Firstov GS, Van Humbeeck J, Koval YuN. Presented at ESOMAT-2003, Cirencester, 17–22 August, 2003, England. Mater. Sci. Eng. A [in press].
[9] Firstov GS, Van Humbeeck J, Koval YuN. J Phys IV Pr8 2001; 11:481–6.
[10] Ortin J, Planes A. Acta Metall 1988;36(8):1873–89.
[11] Meng XL, Cai W, Zheng YF, Tong YX, Zhao LC, Zhou LM. Mater Lett 2002;55:111–5.
[12] Wang YQ, Zheng YF, Cai W, Zhao LC. Scr Mater 1999;40(12): 1327–31.
[13] Mulder JH. Investigation of high temperature shape memory alloys from the Ni–Ti–Zr and Ni–Ti–Hf Systems. Phd. Thesis, University of Twente; 1995. p. 142.
[14] Schryvers D, Firstov GS, Seo JW, Van Humbeeck J, Koval YuN. Scr Mater 1997;36(10):1119–25.